Chemical Research in Toxicology®

Subscriber access provided by Kaohsiung Medical University

Article

Synthesis and Structure Activity Relationship of Pyridazine-Based Inhibitors for Elucidating the Mechanism of Amyloid Inhibition

Hamid R. Kalhor, and Alireza Nazari Khodadadi

Chem. Res. Toxicol., **Just Accepted Manuscript** • DOI: 10.1021/acs.chemrestox.8b00210 • Publication Date (Web): 24 Aug 2018

Downloaded from http://pubs.acs.org on August 25, 2018

Just Accepted

"Just Accepted" manuscripts have been peer-reviewed and accepted for publication. They are posted online prior to technical editing, formatting for publication and author proofing. The American Chemical Society provides "Just Accepted" as a service to the research community to expedite the dissemination of scientific material as soon as possible after acceptance. "Just Accepted" manuscripts appear in full in PDF format accompanied by an HTML abstract. "Just Accepted" manuscripts have been fully peer reviewed, but should not be considered the official version of record. They are citable by the Digital Object Identifier (DOI®). "Just Accepted" is an optional service offered to authors. Therefore, the "Just Accepted" Web site may not include all articles that will be published in the journal. After a manuscript is technically edited and formatted, it will be removed from the "Just Accepted" Web site and published as an ASAP article. Note that technical editing may introduce minor changes to the manuscript text and/or graphics which could affect content, and all legal disclaimers and ethical guidelines that apply to the journal pertain. ACS cannot be held responsible for errors or consequences arising from the use of information contained in these "Just Accepted" manuscripts.

ACS Publications

is published by the American Chemical Society. 1155 Sixteenth Street N.W., Washington, DC 20036

Published by American Chemical Society. Copyright © American Chemical Society. However, no copyright claim is made to original U.S. Government works, or works produced by employees of any Commonwealth realm Crown government in the course of their duties.

Synthesis and Structure Activity Relationship of Pyridazine-Based Inhibitors for Elucidating the Mechanism of Amyloid Inhibition

Hamid Reza Kalhor*, Alireza Nazari Khodadadi

Biochemistry Research Laboratory, Department of Chemistry,

Sharif University of Technology, Tehran, Iran

Corresponding Author:

* Email: kalhor@sharif.edu. Tel: +982166165315. Fax: +982166165315

For TOC only

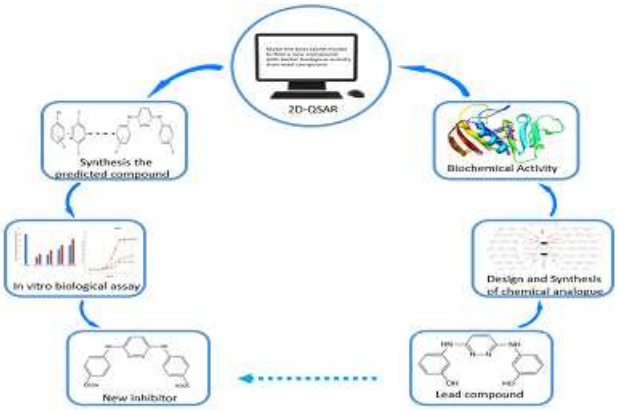
2D-QSAR
Biochemical Activity
Design and Synthesis of chemical analogues
Lead compound
New inhibitor
In vitro biological assay
Synthesis the predicted compound

■ Abstract

Conformational diseases, constituting a large number of diseases, have been connected with protein misfolding, leading to aggregation known as amyloid fibrils. Mainly due to the lack of detailed molecular mechanisms, there has not been an effective drug to combat amyloid-associated diseases. Recently, a small organic pyridazine-based molecule (RS-0406) has shown significant reductions in amyloid fibrils in both in vitro and in vivo animal studies. However, no information on molecular details of inhibition for the small molecule has been reported. In this work, we have decided to explore Structure Activity Relationship (SAR) of pyridazine-based compounds to investigate structural parameters for amyloid inhibition. A number of closely related derivatives of RS-0406 were designed and synthesized to delineate the roles of structural properties, including bulkiness and halogen bonding, hydrogen bonding ability, and the position of substituents on the flanking aromatic rings of the synthetic molecules. To examine the effectiveness of the synthesized compounds, amyloid fibril formation of Hen Egg White Lysozyme (HEWL) was measured in the presence of each synthetic molecule. Our results indicated that in addition to the type of the aryl substituent, their positions on the ring were also important for their inhibitory roles in amyloid fibrils formation. Moreover, a fluorinated compound turned out to be a more effective kinetic inhibitor, displaying a delayed fibril nucleation than the original lead compound. Furthermore, biochemical structural analyses and molecular dynamics simulation revealed that the pyridazine-based compounds may mediate the inhibition of amyloid fibrils through stabilization of the protein monomer during partially unfolded state. The cytotoxicity assay revealed that the amounts of amyloid intermediates were reduced in the presence of the synthetic compounds. Eventually, IC50 values were obtained for the synthetic compounds, and QSAR method was employed to suggest more effective amyloid inhibitors.

Keywords: Protein misfolding, Pyridazine, Amyloid inhibitor, Kinetic inhibitors, Lysozyme, QSAR

■ INTRODUCTION

In order for a protein to gain its native function, it must undergo a folding process. To assist the folding process, a cell exploits a number of ways including molecular chaperons and osmolytes[1–3]. However, in certain conditions, a protein (or a polypeptide) would not fold into its native structure, leading to its misfolding[4,5]. Indeed, the misfolding process has been shown to be accompanied by conformational change in proteins or polypeptides[6]. In humans, a number of conformational diseases have been identified in which misfolded proteins or polypeptides are accumulated as insoluble fibrils; these human debilitating diseases include Alzheimer's, Parkinson, type 2 diabetes, and mad cow[7,8].Neurotoxicity has been shown to be the hallmark of amyloid associated disesases[9]. Amyloid fibrils are unique insoluble, unbranched, and threadlike fibrils with 70–120 Å diameters; since these fibrils are insoluble, it has been difficult to obtain the atomistic details of their structures and interactions with other small molecules[10,11]. However, using solid state NMR, double horseshoe-like (S-shape structure) cross–β-sheet structure in amyloid fibrils has been reported[12,13]. The kinetics of amyloid formation can be divided into three phases; the initial phase, called lag phase, is considered the rate limiting step in which proteins become partially unfolded, leading to nucleus formation upon which other protein monomers are assembled. In the second phase, known as elongation step, the heterogeneous population of soluble oligomers are formed, producing protofibrils, and finally, in the last phase, insoluble amyloid fibrils are formed in the process[14,15]. There exist a number of techniques that can be exploited to detect different stages of amyloid formation including spectroscopic methods to a much simpler approach as gel electrophoresis[16,17]. Proteins and polypeptides that have been used widely as amyloid models include amyloid β-peptide, amylin, insulin, transthyretin, human lysozyme, and Hen Egg White lysozyme (HEWL)[18–21]. HEWL has been used extensively as an

amyloid model mainly due to its well characterized misfolding pathways[22]. HEWL, which mainly possesses alpha helices, can be easily converted to amyloid fibrils at low pH and high temperature (57 °C) during several days. HEWL fibrillation has been highly used to investigate the effects of inhibitors on the physical and chemical process of protein aggregation[23]. In addition, it has been shown that HEWL aggregates can cause neurotoxicity similar to the aggregation of amyloid beta peptide[24].

In the past few years, a number of studies have shown that both natural and synthetic compounds can be exploited to inhibit or reduce amyloid formation[25–29]. In general, the inhibitors fall into two categories: thermodynamic inhibitors which reduce the total amount of amyloid fibrils, and kinetic inhibitors that could extend the time for nucleation of amyloid formation[30,31]. In recent reports in screening of molecular libraries, a pyridazine-based belonging to small organic molecule, coined RS-0406, was identified as an effective amyloid inhibitor both in vitro and animal studies[32,33]. This small organic molecule contains three aromatic rings, with pyridazine as its central ring conjuring up a symmetrical structure with two hydroxyl moieties on the outer rings. Although RS-0406 is now in clinical trial phase II for further considerations, there has not been any report illustrating experimental data on the molecular mechanisms or its biochemical interactions in amyloid inhibition. It has been demonstrated that pyridazine-core compounds play special roles in a number of drugs that interact with proteins. Strong hydrogen bonding ability, high dipolar moment, and higher solubility in water have made pyridazine-based compounds more intriguingly drugs, compared to other diazines[34,35]. In this work, several symmetrical pyridazine-based derivatives, analogous to RS-0406, were synthesized, purified, and characterized by ^{1}H and ^{13}C NMR and HRMS analyses. The synthetic compounds were examined for their effects on amyloid inhibition using Thioflavin-T (Th-T) binding, gel

electrophoresis, and TEM. Furthermore, biochemical effects of the selected synthetic compounds were examined by ANS binding and CD analyses. Moreover molecular dynamics were used to look into the details of interactions between HEWL protein and synthetic compounds. The results illustrated that in addition to the ability of hydrogen-bonding and hydrophobic interactions, the position and the size of substituents play important roles in the inhibition of amyloid formation. Furthermore, a fluorine atom in place of hydroxy group can be more effective as a kinetic inhibitor (the ability to obstruct nucleation of amyloid fibrils). At the end, using the IC50 measurements and the molecular structural descriptors of synthesized compounds, QSAR model was generated; a compound containing carboxylic moiety at the para position of aromatic ring was suggested to possess more inhibitory effect than the lead compound. The predicted compound was synthesized, and when it was examined for its anti-amyloid activity, the compound was not soluble in the acidic medium, and its effect was investigated in alkaline medium.

Materials and Methods

Synthesis of organic compounds:

General information: 3-6-dichloropyridazine was purchased from Sigma Aldrich. All of the other compounds were purchased from Merck, Germany. ^{1}H and ^{13}C NMR spectra were recorded on a Bruker 500 instrument in DMSO-*d6* solvent, With ^{1}H at 500 MHz, and ^{13}C at 125 MHz. ^{1}H and ^{13}C NMR chemical shifts were reported in ppm and were referenced to the residual solvent signals (^{1}H:$(CD_3)_2SO$ at 2.50 ppm, CD_3OD at 3.31 ppm, ^{13}C: $(CD_3)_2SO$ at 39.52 ppm).

General procedure for the synthesis of the pyridazine-based compounds (Py-1 to Py-15)

Synthesis of all compounds was performed in the same setup while applying different methods for isolation and purification. For setting up the reactions, the derivatives of aniline (2-3 eq) were dissolved in 20 mL of 2-ethoxyethanol (2EE) and the solution was stirred at 60 °C for 30 min. Subsequently, 3,6-dichloropyridazine(1eq) was added, and the reaction was refluxed for 18-48 h.

N3, N6-di (3-hydroxyphenyl) pyridazine-3, 6-diamine (Py-1): The reaction was set up according to the general procedure**.** 3-aminophenol (1.10 g) and 3, 6-dichloropyridazine (0.75 g) were used to synthesize Py-1. After 24 h, the solvent was removed by vacuum evaporation. The precipitate was washed with ethanol, dried in an oven, and subsequently purified by column chromatography in (1:1 ethyl acetate/n-hexane) on silica. In a second procedure, the precipitate after evaporation was recrystallized from ethanol, and a few drops of H_2O (less than a milliliter) was added to obtain a brown powder (1.24 g, yield 85%). ^{1}HNMR (DMSO-*d6*, 500MHz): δ 6.59 (d, j=5, 15H), 6.95 (d, j=10, 13H), 7.00(s, 11H), 7.17 (t, j=10, 14H), 7.59 (s, 1H), 9.70 (s, OH),

10.42 (s, 7H). ^{13}C NMR (DMSO-*d6*, 125 MHz): δ108.99, 112.49, 127.79, 127.96, 130.39, 139.62, 150.24, and 159.12. HRMS (ESI^{+}), [M+H]$^{+}$ calcd, 295.1189, found, 295.1189.

N3, N6-di (4-hydroxyphenyl) pyridazine-3, 6-diamine (Py-2): The reaction was set up according to the general procedure**.** 4-aminophenol (1.10 g) and 3, 6-dichloropyridazine (0.75 g) were used to obtain a green powder (1.06 g, yield 72%). After 24 h and before the evaporation of the solvent, ethanol was added drop-wise (the same amount as the volume of solvent) to the mixture of reaction until the crude precipitate was formed. The crude solid was filtered, washed with ethanol and was subsequently recrystallized from acetone. ^{1}HNMR (DMSO-*d6*, 500MHz): δ 6.81(d, j=5, 11H, 15H), 7.30 (bs, 12H, 14H), 7.60 (s, 1H), 9.64 (s, 7H), 10.40 (s, 22H). HRMS (ESI^{+}), [M+H]$^{+}$ calcd, 295.1189, found, 295.1189.

N3, N6-di (3-methoxyphenyl) pyridazine-3, 6-diamine (Py-3): The reaction was set up according to the general procedure**.** M-anisidine (1.2 mL) and 3, 6-dichloropyridazine (0.75 g) were used to obtain a gray powder (1.25 g, yield 78%). After 28 h, the reaction was stopped, and the solvent was removed by vacuum evaporation; the dried precipitate was stirred in basic water (NaOH 1.25 M) containing a few drops of acetone for 1h. Subsequently, the solution was centrifuged at 400 rpm for 5 min. The precipitate was recrystallized from acetone. ^{1}HNMR (DMSO-*d6*, 500MHz): δ 3.75 (s, OCH_3), 6.48(d, j=5, 15H) 7.12(s, 11H), 7.18(t, j=15, 13H), 7.26(d, j=10, 14H), 7.42 (s, 4H), 9.00 (s, 7H). ^{13}C NMR (DMSO-*d6*, 125 MHz): δ 55.99, 104.67, 106.50, 111.33, 121.36, 130.47, 143.88, 153.33, and 160.85. HRMS (ESI^{+}), [M+H]$^{+}$ calcd, 323.1502, found, 323.1503.

N3, N6-diphenylpyridazine-3, 6-diamine (Py-4)[36]: Following the same procedure for the synthesis of Py-3, aniline (1 mL) and 3, 6-dichloropyridazine (0.75 g) were used to obtain a yellow powder (0.74 g, yield 57%). ^{1}HNMR (DMSO-*d6*, 500MHz): δ 7.15(t, j=15, 13H), 7.40(t, j=15, 12H, 14H), 7.57 (d, j=10, 11H, 15H), 7.78 (s, 4H), 10.72 (s, 7H).^{13}C NMR (DMSO-*d6*, 125 MHz): δ 121.897, 125.212, 127.696, 130.363, 138.978, 150.348. HRMS (ESI^{+}), [M+H] $^{+}$ calcd, 263.1291, found, 263.1291.

N3, N6-di (4-bromophenyl) pyridazine-3, 6-diamine (Py-5): Following the same procedure for the synthesis of Py-3, in a similar scale, a gray powder (1.42 g, yield 68%) was obtained after 48 h. ^{1}HNMR (DMSO-*d6*, 500MHz): δ 7.14(s, 4H), 7.46(d, j= 10, 11H, 15H), 7.75 (d, j=10, 12H, 14H), 9.21(s, 7H). ^{13}C NMR (DMSO-*d6*, 125 MHz): δ 112.40, 120.61, 121.81, 132.45, 141.85, 153.03. and 153.426. HRMS (ESI^{+}), [M+H] $^{+}$ calcd, 418.9501, found, 418.9499.

N3, N6-di (3,4-dichlorophenyl) pyridazine-3, 6-diamine (Py-6): Applying the same procedure for the synthesis of Py-3**;** 3,4- dichloroaniline (2.00 g) and 3,6-dichloropyridazine(0.75 g) were used to obtain a brown powder (1.10 g, yield 55%) in 48 h. 1HNMR (DMSO-*d6*, 500MHz): δ 7.15(s, 1H), 7.49(d, j=10, 15H), 7.62 (d, j=10, 14H), 8.25 (s, 11H), ^{13}C NMR (DMSO-*d6*, 125 MHz): δ 118.806, 119.373, 121.803, 122.105, 131.470, 131.934, 142.647, and 153.200. HRMS (ESI^{+}), [M+H] $^{+}$ calcd, 398.9732, found, 398.9737.

N3, N6-di (3-fluorophenyl) pyridazine-3, 6-diamine (Py-7). Synthesis of Py-7 was set up according to the general procedure. 3-fluoroaniline (1 mL) and 3, 6-dichloropyridazine (0.75 g) were used to give a yellow powder (0.44 g, yield 29%) in 48 h. The precipitate after vacuum evaporation was stirred in 20 mL NaOH (1.25 M), without acetone. The precipitate was

extracted using centrifugation (400 rpm for 5 min). Subsequently, the precipitate was dried and recrystallized from acetic acid or purified by column chromatography in (3:1:0.1 ethyl acetate: n-hexane: acetic acid) on silica. ^{1}HNMR (DMSO-*d6*, 500MHz): δ 6.95(t, j=15, 14H) 7.34(d, j=5, 15H), 7.43(q, j=25, 13H), 7.64(d, j=10, 11H), 7.80(s, 1H), 11.00(s, 7H). ^{13}C NMR (DMSO-*d6*, 125 MHz): δ 117.60, 127.38, 131.87, 141.87, 150.40, 162.47, and 167.49. HRMS (ESI^{+}), $[M+H]^{+}$ calcd, 299.1102, found, 299.1102.

N3, N6-di (3-nitrophenyl) pyridazine-3, 6-diamine (Py-8): Following the procedure for the synthesis of Py-3, at the same scale, a dark brown powder (0.54 g, yield 30%) was obtained after 48 h. ^{1}HNMR (DMSO-*d6*, 500MHz): δ 7.23(s, 1H), 7.59 (t, j=15, 14H), 7.75 (d, j=5, 15H), 8.08 (d, j=10, 13H), 8.86 (s, 11H), 9.66 (s, 7H). ^{13}C NMR (DMSO-*d6*, 125 MHz): δ 112.300, 115.697, 121.954, 124.678, 121.053, 143.670, 149.358, and 153.426. HRMS (ESI^{+}), $[M+H]^{+}$ calcd, 353.0992, found, 353.0993.

N3, N6-di (3-chlorophenyl) pyridazine-3, 6-diamine (Py-9): Following the same procedure for the synthesis of Py-3, at the same scale, a gray powder (0.33 g, yield 20%) was obtained after 48 h. ^{1}HNMR (DMSO-*d6*, 500MHz): δ 6.91(d, j=10, 15H) 7.22(s, 1H), 7.29(t, j=15, 14H), 7.58(d, j=10, 13H), 8.08(s, 11H), 9.63(s, 7H). ^{13}C NMR (DMSO-*d6*, 125 MHz): δ 116.87, 117.67, 120.37, 121.65, 131.33, 134.04, 144.20, and 153.15. HRMS (ESI^{+}), $[M+H]^{+}$ calcd, 331.0511, found, 331.0510.

N3, N6-di (4-chlorophenyl) pyridazine-3, 6-diamine (Py-10): Following the procedure for the synthesis of Py-3, at the same scale, gray powder (0.74 g, yield 45%) was obtained after 48 h. ^{1}HNMR (DMSO-*d6*, 500MHz): δ 7.11(s, 1H), 7.31(d, j=15, 11H, 15H), 7.79(d, j=15, 12H, 14H),

9.14(s, 7H). ^{13}C NMR (DMSO-*d6*, 125 MHz): δ 120.03, 121.38, 124.24, 129.53, 141.47, and 153.04. HRMS (ESI^{+}), $[M+H]^{+}$ calcd, 331.0511, found, 331.0509.

N3, N6-di (4-methyl benzoate) pyridazine-3, 6-diamine (Py-11): Methyl 4-aminobenzoate was synthesized from 4-aminobenzoic acid in the presence of methanol and thionylchloride[37]. The reaction was set up according to the general procedure**.** Methyl 4-aminobenzoate (1.5 g) and 3, 6-dichloropyridazine (0.75 g) were used to obtain a light brown powder (0.47 g, yield 25%). After 48 h, the reaction was stopped, and the solvent was removed by vacuum evaporation; the viscous sediment was washed in methanol. The methanol was omitted with a syringe, and the precipitate was washed several times with methanol; subsequently, the precipitate was dried and recrystallized from methanol containing a few drops of H_2O. ^{1}HNMR (DMSO-*d6*, 500MHz): **^{1}HNMR** (DMSO-*d6*, 500MHz): δ 3.83(s, 30H).7.68 (s, 1H), 7.78(d, j=5, 11H, 15H), 7.95(d, j=10, 12H, 14H), 10.64(s, 7H). ^{13}C NMR (DMSO-*d6*, 125 MHz): δ 52.00, 116.88, 120.87, 130.65, 146.16, 152.39, and 166.77. HRMS (ESI^{+}), $[M+H]^{+}$ calcd, 379.1400, found, 379.1400.

N3, N6-di (4-nitrophenyl) pyridazine-3, 6-diamine (Py-12): The reaction was set up according to the general procedure**.** 4-nitroaniline (1.5 g) and 3, 6-dichloropyridazine (0.75 g) were used to obtain an orange powder (0.53 g, yield 30%). After 18 h, the reaction was stopped and it was allowed to cool off. Afterwards, using filter paper, the solvent was removed. The precipitate was washed with ethanol and NaOH (1.25M); the precipitate was collected and dried in an oven, and it was recrystallized from methanol containing a few dross of NaOH (1.25M). . ^{1}HNMR (DMSO-*d6*, 500MHz): δ 7.33 (s, 1H), 7.96(d, j=10, 11H, 15H), 8.24 (d, j=10, 12H, 14H), 10.02(s, 7H). ^{13}C NMR (DMSO-*d6*, 125 MHz): δ 117.05, 117.44, 121.57, 139.73, 148.33, and 152.88.

N3, N6-di (4-fluorophenyl) pyridazine-3, 6-diamine (Py-13): Following the procedure for synthesis of Py-7, at the same scale, a dark yellow powder (0.23 g, yield 15%) was obtained after 48 h. ^{1}HNMR (DMSO-*d6*, 500MHz): δ 7.11 (t, j=20 12H, 14H), 7.20 (s, 1H), 7.80(d, j=5, 11H, 15H), 9.30(s, 7H).. ^{13}C NMR (DMSO-*d6*, 125 MHz): δ 115.14, 119.14, 120.04, 138.22, 152.17, and 156.16. HRMS (ESI^{+}), [M+H] $^{+}$ calcd, 299.1102, found, 299.1105.

N3, N6-di (3-methylphenyl) pyridazine-3, 6-diamine (Py-14): Applying the same procedure for synthesis of Py-3, at the same scale, a gray powder (0.56 g, yield 39%) was obtained after 48 h. ^{1}HNMR (DMSO-*d6*, 500MHz): δ 2.24(22H), 6.70(d, j=5, 13H), 7.09(s, 11H), 7.16(t, j=15, 14H), 7.52(d, j=10, 15H), 8.84(s, 1H), 9.63(s, 7H), ^{13}C NMR (DMSO-*d6*, 125 MHz): δ 21.87, 115.22, 118.36, 120.60, 121.34, 128.97, 138.13, 142.12 and 152.67. HRMS (ESI^{+}), [M+H] $^{+}$ calcd, 291.1604, found, 291.1601.

N3, N6-di (4-benzoic acid) pyridazine-3, 6-diamine (Py-15): Py-11 (0.3 g) was dissolved in 5 mL DMSO; an aqueous solution of LiOH (0.65M) was added drop-wise as the same volume of DMSO. After 24 h, the reaction was stopped by adding 20 mL of H_2O and 5 mL of diethyl ether; HCl were used to adjust pH of the aqueous phase (pH 2). Finally, the aqueous phase was saturated with $CHCl_3$. The brown solid precipitate was filtered (0.28 g, yield 93%). In a second method which was similar to the synthesis of Py-12, with the only difference that NaOH was not used for purification. ^{1}HNMR (D_2O, 500MHz): δ 6.80 (s, 1H), 7.25(d, 11H, 15H), 77.60(d, 12H, 14H), ^{13}C NMR (D2O, 125 MHz): δ 117.11, 121.97, 128.91, 130.05, 143.00, 125.18, and 175.35. ^{1}HNMR (DMSO-*d6*, 500MHz): 7.69 (d, j=10, 11H, 15H), 7.84 (s, 1H), 7.96 (d, j=10, 12H, 14H), 11.00 (s, 7H), broad peak in 12.00 (carboxylic acid proton), ^{13}C NMR (DMSO-*d6*, 125 MHz): 119.76, 125.75, 126.59, 131.20, 142.69, 150.13, 162.60. HRMS (ESI^{+}), [M+H] $^{+}$

calcd, 351.1087, found, 351.1088. IR (KBr) ν (cm−1), for Py-11(Ester): 3330 (ν, NH), 2950 (ν, C-H), 1700 (ν, C=O), and for Py-15(Acid): 2600-3500(ν, OH), 1630 (ν, C=O).

Preparation of stock solution from organic compounds

All the synthetic compounds were dissolved in DMSO to the final concentration of 13900 μM and then they were diluted with buffer to the specific final concentration.

Sample preparation for amyloid fibril formation:

Acidic condition: Solutions containing HEWL (349 μM) and the synthetic compound (349 μM) were prepared in 100 mM of glycine buffer at pH 2.5. The solution was incubated at 57 °C for 10 days; samples were taken out every 24 h and stored at -20 °C for further analysis. DMSO (2.5 % v/v) was used for dissolving the synthetic compounds in aqueous medium and thus a sample containing 2.5% DMSO as a control was employed to determine whether DMSO itself had an effect on the HEWL aggregation.

Basic condition: HEWL fibril formation in the basic medium was prepared as previously reported[38]. Briefly, HEWL (349 μM) was incubated for 14 h at 25-28ºC with 3 fold molar of the synthetic compounds in phosphate buffer (10 mM pH 7.3). The incubated samples diluted 3 fold with phosphate buffer (50 mM, pH 12.2) to induce the aggregation of HEWL. Then the solution was incubated at 25-28 °C for 10 days.

Thioflavin T fluorescence Assay: For Th-T fluorescence intensity analysis; 15 μL from aliquoted samples and 185 μL from stock solution of Th-T in sodium phosphate (NaH_2PO_4 50 mM, Na_2HPO_4 50 mM, Th-T 18μM) was mixed; subsequently, measurements were performed

by exciting wavelength at 440 nm and emission wavelength at 485 nm using Synergy H4.To check the error bar, tree independent experiment were used for each inhibitor[39]

IC50 calculation: IC50 values were determined in two ways. In the first method, the Th-T fluorescence assay was performed at 7 concentrations (1nM to 1mM) for each inhibitor and 2mg/mL HEWL in two or three independent experiments for each concentration of inhibitors. The IC50 values were obtained from dose−response curves. In the second method the IC50 values were determined with QSAR method[40,41].

Agarose gel electrophoresis: The procedure was performed as explained in details elsewhere[39]. Briefly, 1% agarose gel using 0.1% SDS in buffer A (200mM Tris and 200mM glycine) was prepared. The gel was run at 70 V for 2 h in buffer A containing 0.1 % SDS. The gel was stained by Coomassie Brilliant Blue for 2 h and destined over nigh in destining solution.

Circular Dichroism (CD): HEWL samples were diluted in the final concentration 0.2mg/mL in glycine buffer 100 mM and pH 2.5; then spectra were recorded from 190 to 260 nm (far-UV) using CD spectrometer Aviv, USA model-125 and 1 mm path cell at room temperature. Spectra for buffer without and with synthetic compounds at the same concentration were recorded.

ANS Fluorescence Assay: A stock solution of ANS was prepared at 0.01M by dissolving ANS in absolute ethanol and filtered using a 0.2 μm cellulose filter. A final solution 100mM was diluted by deionized water.). For ANS fluorescence intensity analysis; 10 μL from aliquoted samples and 200 μL from 100mM stock solution was mixed, and subsequently, measurements were obtained by excitation wavelength at 365 nm and emission spectra at 430 to 550 nm.

Transmission Electronic Microscopy (TEM): Samples were diluted 5 fold by absolute ethanol; subsequently 10 μL of the diluted sample were placed on a copper 300 mesh grid, covered with

carbon-coated formvar film. After a few minutes, the grids were washed with deionized water then stained with 1% (w/v) uranyl acetate, and the grid was incubated 30 min at room temperature for drying. The prepared grids were viewed using Philips CM300 instrument at a voltage of 80kV.

MTT cell viability assay: The PC12 cell (as a model for neurosecretion cells), obtained from Stem Cell Technology Center (Bonyakhteh, Tehran, Iran). The viability of PC12 cells was determined using the MTT assay. The cells were cultured in DMEM (high glucose) medium, supplemented with penicillin-streptomycin (Pen-Strep) 100U/mL and incubated at 37˚C in a 5% CO_2 humidified atmosphere. For cytotoxicity assay, HEWL native, synthetic compounds, and aliquots incubated samples (fibrillation of HEWL in absence and presence of any synthetic compound) were added to the cells (in a final concentration of 20 μM) and incubated in the 48-well plates for 24 h. Subsequently, 25 μl of MTT (from stock 5 mg/mL in PBS) were added to 250 μl of medium and incubated for 3 h. Finally, cells were treated with DMSO (10 min) and absorbance was measured at 570 nm.

Docking and molecular dynamics simulation: The structure of HEWL protein was downloaded from Protein Data Bank online server (PDB ID: 1AKI). The structures of the small molecules were obtained from PRODRG 2.x online server. In order to assemble protein-small molecule complexes, the small molecules were docked to the protein using Auto Dock Tools 1.5.6 software. The resulting complexes as well as HEWL protein with no small molecule as a control system, were subjected to molecular dynamics simulations using GROMACS package. The OPLSaa force field was chosen; in each case, hydrogen atoms were added and titrable residues were protonated corresponding to pH 2; the disulfide bonds of Cysteine residues were in non-reduced form. The protein (with or without small molecule) was centered in a cubic box

with faces at least 1.0 nm apart from the closest atom of the protein. The resulting systems were solvated by SPC216 water and neutralized by adding sufficient amount of ions; in addition, further ions pairs (Na^+ and Cl^-) were added to reach the ionic concentration of 0.1 mol/L. Each system was energy minimized by the steepest descent integrator and emtol value of 100.0 kJ/mol/nm. After minimization, 100 ps equilibration under NVT ensemble was carried out by leap-frog integrator, the temperature was set at 331 K. Furthermore, 100ps equilibration under NPT ensemble was done using leap-frog integrator, in which temperature and pressure were at 331K and 1.0 bar respectively. In each equilibration steps, position restraints on protein and the small molecule atoms were applied. Then, the systems were simulated under NPT ensemble with no position restraints and at the same temperature and pressure. The simulation time was 40ns in each case. In all equilibration and MD simulation steps, integration time was assigned to be 2fs, for equilibrations, velocities, coordinates, and energies were saved every 1.0ps and for MD simulation, energies were saved every 10.0 ps. All bonds were constrained using Links algorithm. Short range electrostatic and Van der Waals interactions were updated every 20fs (10*2fs) with varlet cutoff scheme, the cutoff value was 1.0nm for equilibrations and 1.4nm for MD simulation. Long range electrostatic interactions were calculated using PME method with 0.16 Fourier spacing value. Temperature couplings have been done by V-rescale method with a 0.1ns time constant and pressure couplings have performed by Parrinello-Rahman method with 2ps time constant.

QSAR method: The compounds of constituents of the database optimized in Gaussian03 and Spartan. All of the molecular descriptors were obtained with PaDel program. The most effective and optimal descriptors selected with Genetic Algorithm (GA) software, and finally chemoface software was used to make a valid model and prediction of IC50[40,41].

■ RESULTS

Design of synthetic molecules

To better investigate the mechanism of amyloid inhibition by pyridazine-based inhibitors, a number of derivatives of RS-0406 were rationally designed and synthesized. To study the role of hydrogen-bonding, the hydroxyl substituent on the lead compound (Py-1) was replaced with methoxy (Py-3), fluorine atom (Py-7), nitro (Py-8), or no substitution (Py-4), (Table 1). To compare the role of meta (C12) versus para (C13) position on aryl rings, compounds containing hydroxyl moiety (Py-1/ Py-2), fluorine (Py-7/ Py-13), chlorine (Py-9/ Py-10), and nitro moiety (Py-8/Py-12) were designed (Table 1). To probe the role of bulkiness and halogen-bonding, four halides containing compounds: Py-13, Py-5, Py-10, and Py-6, were designed (Table 1). Because of the symmetrical structure of the lead compound (RS-0406), all other synthesized compounds in this work were also kept symmetrical.

Synthesis of pyridizine-based compounds

Py-1 was identified in screening of a large number of organic compounds, and so there has not been any actual report on its synthesis except a patented document[42]. The synthesis of this compound and their derivatives, as explained in details in the Materials and Methods section, was performed without using any chemical catalyst or a base. Several solvents were examined for the yield optimization of reactions including, DMF, DMSO, HMPA, and 2-ethoxy ethanol (2EE); as a result, 2-ethoxy ethanol turned out as the best solvent. The synthesis of symmetrical products indicated that the highest yields pertained to Py-1, Py-2 and Py-3, and the rate of reaction for synthesis of Py-12 was the highest. After purification, a number of analytical

techniques were employed for characterization of the products including ^{1}H and ^{13}C NMR, and HRMS, as shown in Fig. S1-S15.

In vitro biological activity of pyridazine-based compounds in amyloid inhibition

In order to study the biological role of the synthesized compounds, in vitro amyloid fibril formation was performed in the presence of the synthetic compounds. In this assay, HEWL is converted to amyloid fibril at low pH and high temperature. The amount of Thioflavin-T (Th-T) fluorescence reflects the amounts of fibril produced during the course of reaction; that is, the more protein fibrils are produced, the more Th-T molecules are bound to the fibrils, leading to more fluorescence emission. As shown in Fig. 1A, the compound Py-1, containing hydroxyl moiety at meta position (C12), displayed the most inhibitory effect thermodynamically; the next best inhibitor was identified as Py-7 which contains fluorine in place of hydroxyl group. The worst inhibitor (for the role of hydrogen bonding), turned out to be a compound Py-8. In general, as the substituent on the aryl ring became bulkier, the amyloid inhibitory effect of the compound became weaker (Fig. 1B); However, Py-5 (containing bromine), was more effective than Py-10 (containing chlorine), in inhibiting the amyloid formation. The compounds containing substitution in meta (C12) versus para (C13) position on the aryl ring were investigated by several functional groups such as hydroxyl, fluorine, chlorine, and a nitro moiety (Fig. 1C). Interestingly, all of the compounds which possess a meta moiety (C12) displayed more pronounced inhibitory effects than those containing a para moiety (C13) (Fig. 1C). The kinetic studies of the synthesized compounds were also performed (Fig. S19). Interestingly, Py-7, containing fluoro-moiety, thermodynamically inhibited amyloid formation near 70 % and delayed the aggregation process up to 125 h; in other words, Py-7 seems to be a more effective in extending the lag time for nucleation of amyloid fibrils than Py-1(Fig. 1D).

In order to actually detect the intermediates in the process of amyloid formation, gel electrophoresis was performed; the gel electrophoresis can be very informative about the three phases of amyloid fibril formation. Amyloid fibrils, due to their large size, are mostly retained in agarose gel well during electrophoresis whereas heterogeneous population of soluble oligomers are spread out as smears; the native protein (as a monomer) can be detected as a single band[17]. When examining the amyloid fibrils intermediates, the amount of fibril in the absence of inhibitors was higher than in the presence of inhibitors, confirming the Th-T binding assay (Fig. S16).

To better confirm amyloid inhibition mediated by the synthetic compounds: Py-1 (the most effective inhibitor), Py-6 (the least effective inhibitor) and Py-7 were selected for TEM analysis. In the absence of any synthetic compound, fibril formation was abundant; the sizes of fibrils were estimated to be 20-30 nm; however, in the presence of Py-1 the fibrils were immensely reduced (Fig. 2A and 3C). In the presence of Py-6, the amount of fibril was not reduced significantly compared to the control (Fig. 2B). Interestingly, in the presence of Py-7, not only the amount of amyloid fibrils was reduced but also the presence of substantial low molecular weight was detected; these particles may represent either nucleus or oligomers that did not convert to amyloid fibril (Fig. 2D).

Protein structural analysis

The effects of synthesized compounds on the secondary structure of HEWL was examined using Circular Dichromism (CD). As seen in Fig. 3A, the secondary structure of native HEWL in the absence of any synthetic compound (control) were detected as mostly alpha helices, at the beginning of amyloid process. However, at the late stage of amyloid formation, a remarkable

conformational change, from alpha helix (at 208 and 222 nm) to the beta sheet (217 nm) was observed. In the presence of Py-1, the conformational change to beta sheet was not seen as it was observed in the control, displaying higher alpha helices at the late stage of amyloid formation (Fig. 3B). However, the high content of alpha helix was not observed with Py-6 whereas in the presence of Py-2 the content of alpha helices of the protein was nearly conserved, but not as efficient as in the presence of Py-1, during the late stage of amyloid formation. The CD analysis confirmed the importance of position of substituent for the inhibitory ability of Py-1 and Py-2 in amyloid fibril formation (Fig. 3C and Fig. 3D). Additionally, few signals were also observed in the presence of synthetic compounds between 190-200 nm, demonstrating significant changes in secondary structure of the protein during amyloid fibrillation; these secondary structural changes have been reported in the previous studies[43].

To investigate the hydrophobic exposure of protein core during amyloid formation, ANS binding of HEWL was measured in the absence and presence of synthetic compounds. Generally, as proteins become unfolded, during the misfolding process, more hydrophobic core of the proteins is exposed; therefore, more ANS binding can occur, leading to the emission of more fluorescence intensity. The ANS binding experiments indicated that as amyloid formation progressed, in the absence of any synthetic compound, more ANS fluorescence was observed due to increased binding of ANS to the hydrophobic regions of HEWL (Fig. S17A). In the presence of synthetic compounds, a reduction of ANS fluorescence was detected for Py-1, Py-2, and Py-4. However, ANS fluorescence in the presence of Py-6 displayed little reduction in the fluorescence emissions (Fig. S17B). These results not only confirmed the Th-T binding assay, but they also indicated that the protein structure in the presence of synthetic compounds was less unfolded and exposed to the environment, giving rise to less amyloid fibril.

Cytotoxicity of aggregated HEWL in the presence of pyridazine- based compounds

To gain more insight into the effects of the synthesized compounds on cytotoxicity of amyloid intermediates, the viability of PC12 cell line (a neuron model cell line) was examined using MTT assay. The amyloid formation assay was performed in the presence of various synthetic compounds, and subsequently the mixtures, along with control sample lacking any synthetic compound, were incubated with PC12 cells. As shown in Fig. 4A, while no cytotoxicity was observed for HEWL native, HEWL amyloid fibrils reduced the percentage of cell viability, indicating that amyloid intermediates were toxic to cells. The HEWL samples that were incubated in the presence of Py-1, Py-2, and Py-7 displayed higher cell viability than other compounds, corroborating the Th-T binding assay. Morphological changes of PC12 cells also confirmed the protective effect of pyridazine-based compounds on cytotoxicity of aggregated HEWL (Fig. 4B).

Docking and MD analysis of synthetic compounds

In order to better investigate the details of molecular interactions of the synthetic compounds and HEWL, molecular dynamic simulation was performed. Initially, Py-1, Py-7 and Py-4 were docked onto HEWL, and simulations were carried out at high temperature and low pH (resembling the experimental amyloidogenic conditions). RMSD results showed that in the presence of Py-1, HEWL became more stable as compared to other two compounds (Fig. 6A and 6B). Interestingly, both Py-1 and Py-7 displayed significant noncovalent interactions with amino acid residues that are located in the amyloidogenic region of HEWL, including hydrophobic cluster 57-107 with Trp61 residue[44,45]. The types of interactions that Py-1 and Py-7 formed with HEWL included hydrophobic, hydrogen-bonding and van der Waals interactions (Fig. 6C and

Fig. 6D). The interactions of docked Py-4 lacking hydroxyl group was performed for comparison with the control, but RMSD for Py-4 showed not much difference with the control (Fig. 6B).

Applying QSAR method for obtaining more effective inhibitors

Since some of the synthetic compounds have shown anti-amyloid activities close to the original lead compound, one meaningful approach would be exploiting the pyridazine-based amyloid inhibitors to perform QSAR. IC50 inhibitory effects of the synthetic compounds were measured (Table 2). A best QSAR model was created using IC50 values (R^2= 0.966, RMSE=0.146). Py-15 containing carboxylic group was predicted to display more potent IC50 (smaller IC50) than the original compound (Table 2). Therefore, Py-15 was synthesized, purified and confirmed as described in the Materials and Methods section and in Fig. S15. When amyloid assay was performed, in the-presence of Py-15 the compound was precipitated out due to highly acidic condition of the assay.

■ DISCUSSION

Due to the physicochemical properties of pyridazine, pyridazine-based compounds have been used widely in drug-protein interactions[35,46]. However, limited pyridazine-based compounds have been introduced as amyloid inhibitors. RS-0406 has recently been reported as an important amyloid inhibitor[32,33]; the mechanism of the amyloid inhibition has been largely missing. In this study, a number of related compounds were synthesized in order to gain more mechanistic information on the inhibition of amyloid by pyridazine-based compounds and also to make a data set of RS-0406 analogs for finding a better amyloid inhibitor. The pyridazine-based compounds were synthesized using amination reactions without using any catalyst or base (Table 1). It is worth mentioning that the electrophile (3, 6-dichloropyridazine) must be added after dissolving the nucleophile (aniline derivatives); otherwise, there could be little products mainly due to high dipole momentum (3.9 D) of pyridazine which is generated by two nitrogen atoms adjacently positions in its ring[47]. Additionally, the solvent (2EE) used in the reaction, also possesses a high dipole moment (2.08 D); if both solvent and reactants were added simultaneously, the nucleophilic substitution reaction would most likely be hindered. Nucleophilic substitution at carbons of the pyridazine ring occurs by addition-elimination (S_NAr) mechanism. Both the leaving group (chlorine atom) and the nucleophile (Ar-NH2) have-determinant roles in -the reaction mechanism. Since, in this work, no chemical catalyst or a base was used to synthesize novel compounds, rate and the yield of reaction was mainly dependent on the leaving group, Ar-NH_2 substituent, temperature, and solvent. All of the compounds were synthesized in the same solvent and temperature; therefore, substituent of Ar-NH_2 played a key role in the synthesis of pyridazine-based compounds. A four-step mechanism has been proposed

for the synthesis of Py-1 to Py-15, indicating the rate determining step as disruption of pyridazine aromaticity (Fig. S20). The synthesis of symmetrical products indicated the highest yields pertained to Py-1, Py-2, and Py-3 which contain the electron-donor moiety as an activator in the first step of reaction. Interestingly, the synthesis of Py-12 performed in 18 h and the product was precipitated out in the mixture of reaction. Further looking into the effects of substituent of Ar-NH_2, Mulliken atomic charge on chlorine (leaving group) was calculated (Fig. S20). In fact, a nitro group, in para position to -NH- (Py12), was partially blocked from electron donation from -NH- to pyridazine ring, resulting in a faster reaction during the slowest step of the reaction (third step).

The results demonstrated that several structural parameters including hydrogen bonding, position of the aromatic substituent, and bulkiness (halogen-bonding ability) most likely are involved in inhibition of amyloid by the pyridazine-based compounds. Most notable factor, based on our results, is the position of the substituent on the outer aromatic rings of the synthetic compounds (Fig. 1C). To better understand the position effect, the optimized structures of synthetic compounds were compared using Gaussian[48]. It was revealed that the para-substituted compounds of the library were all entirely flat as compared to their meta counterparts (Fig. 5). Therefore, it could be reasoned that the lesser inhibitory effect of para substituted compounds might be related to their inability to finely tune to interact with the protein during unfolding process. Indeed, Py-15 which has para carboxyl substitution was predicted to have a better inhibitory effect than its meta counterpart. However, its optimized structure revealed a lack of flat structure, similar to the other meta substituent compounds, as opposed to its flat meta counterpart (Fig. 5).

The cytotoxicity effect of protein aggregate in the presence of the synthetic compounds indicated that those compounds that displayed less Th-T binding assay also caused less toxicity at the cellular level (Fig. 4). Interestingly, Py-7 displayed more cell viability than original lead compound (Py-1). This difference might be due to more toxicity of oligomers than the amyloid fibrils that have been reported previously[49] and perhaps Py-7 prevented oligomer formation more effectively as supported by its longer lag time in Th-T binding assay and gel electrophoresis. It must be noted that toxicity and the amount of amyloid fibrils formed are not always correlative where an inhibitor might increase fibril formation but reduce toxicity[50].

In the absence of any crystal structure of the amyloid forming protein (HEWL) in the presence of the pyridazine-based inhibitors, it can be suggested that a hydroxyl group on the aryl ring, as in Py-1, can be very effective to inhibit amyloid formation. However, when the hydroxyl group is in para position, the inhibitory effect is reduced. Since anti-amyloid properties of several compounds have been linked to their antioxidant effects, Bond Dissociation Energy (BDE) has been used as a parameter to compare antioxidant potency[51–53]. Interestingly, when BDE was calculated for both Py-1 and Py-2, the meta substituted compound (Py-1) displayed a lower BDE (Fig. S18), therefore, Py-1 can potentially act as an antioxidant more effectively than Py-2. Interestingly, when the hydroxyl groups were completely removed (as in Py-4), amyloid inhibition was significantly reduced; however, the amyloid formation was not completely prevented most likely due to the presence of pyridazine ring and hydrogen-bonding between the amino group of the inhibitor and the protein (Fig. 6B). In a very recent study, a molecular dynamics studies using Py-4 and Py-1 against Abeta peptide oligomer indicated the role of the hydrogen-bonding in pyridazine-based inhibitors[54].

Compound Py-8 containing two nitro groups also displayed much less inhibiting effect than all the synthetic compounds that were studied for their hydrogen bonding abilities (Fig. 1A). Although the nitro moiety is capable of making hydrogen-bonding, it could also reduce the solubility of organic compounds in aqueous solution. Indeed, indole-based compounds containing nitro groups have shown much less inhibitory effects[55]. Noncovalent protein-ligand interactions have been shown to be influenced by halogens through halogen bonding and hydrogen-bonding[56]. A halogen-bond is defined as a noncovalent bond between a halogen atom, (Cl, Br, and I substitution of ligand) as a Lewis acid, and an electron donor, (Nitrogen and Oxygen in backbone of protein) as a Lewis base. However, fluorine cannot form a halogen bond due to its high electronegativity and inability to interact with nucleophiles[56–58]. Realizing that in the present work Py-5, containing bromo-moiety, turned out to be more effective amyloid inhibitor than Py-9 and Py-10, this effect may be explained mainly by more halogen bonding ability of bromine than chlorine atom since halogen bonding is enhanced with the increasing in size of halogen atom. However, Py-6, containing two chloro moieties, displayed less inhibitory effect than Py-9 and Py-10 which both contain one chloro moiety. Therefore, a bulkier ligand can have weaker interactions with proteins due to its steric effect. In addition, the compound containing fluoro (Py-7) can exert a similar effect as the hydroxyl group in Py-1 because organic fluorine substitution is small and capable of making hydrogen-bonding[59]. In molecular dynamic simulation, RMSD values indicate stabilization of protein ligand complex. The RMSD trajectory of HEWL/Py-1 complex demonstrated that with the progress in simulation the complex became more stable than complexes of HEWL/ Py-4 and HEWL/Py-7, confirming the effectiveness of interactions between the Py-1 and -HEWL. More interestingly, when the interactions of small synthetic compounds during simulation were analyzed, both Py-1 and Py-7 demonstrated

noncovalent interactions such as hydrogen bonding and π-π interaction (parallel and vertical) with residues in the amyloidogenic region of HEWL.

To generate a reasonable QSAR model, the pyridazine-based compounds that were synthesized in this study were employed in a library in such a way that most of the compounds in the library would have a similar pharmacophore, making the prediction more reliable[60]. In addition, the IC50 values were measured for most of the pyridazine-based compounds (Py-1 to Py-11). Using the measured IC50 values, a model was built; subsequently, among a number of suggested pyridazine-based compounds, the model predicted that Py-15 as more effective than the original lead compound (Table 2). Interestingly, the predicted compound (Py-15) which possesses a para carboxy moiety, were predicted to have a lower IC50 than its meta counterpart (Py-16). However, when the two compounds were compared structurally, Py-15 displayed a non-planer structure similar to the other meta substituted compounds as opposed to its meta counterpart (Fig. 5). We have also examined the effect of Py-15 as an amyloid inhibitor under non-acidic condition due to low solubility of the compound in low acidic medium. The results did not match the QSAR prediction most likely due to a different condition (low pH) that the model was built upon.

Supporting Information Available: Figures S1-S15 includes NMR spectra analysis for synthetic compounds (Py-1- Py-15). Fig. S16 shows gel electrophoresis of aggregation assay in the absence and presence of inhibitors. Fig. S17 ANS binding assay HEWL in absence and presence of inhibitor. Fig. S18 demonstrates BDE of hydroxyl moiety on Py-1 and Py-2, and Fig. S19 depicts kinetic studies of pyridazine-based compounds. Fig. S20 Proposed mechanism for the syntactic compounds.

Funding Sources: This work was partially supported by Sharif University of Technology grant (G930614).

Acknowledgments

We would like to thank Parsa Jabbari for his assistance in molecular dynamics simulations. We are immensely grateful to Professor Xiuling Cui (Zhengzhou University) for his assistance in HRMS. We are also thankful to Dr. Reza Kia (Sharif University of Technology) for assistance in 2D NMR.

Abbreviations

HEWL, hen egg white lysozyme; ANS, 8-anilino-1-naphthalenesulfonic acid; Th-T, thioflavine-t; SDS, sodium dodecyl sulfate; DMF, dimethylformamide ; DMSO, dimethyl sulfoxide; HMPA, hexamethylphosphoramide; 2EE, 2-ethoxy ethanol; 3-(4,5-dimethyl tiazol-2-yl)-2,5 diphenyl tetrazolium bromide; HRMS, high resolution mas spectroscopy; NMR, nuclear magnetic resonance; TEM, transmission electron microscopy; CD, circular dichroism; MD, molecular dynamic; RMSD, root-mean-square deviation; RMSE, root-mean-square error; QSAR, quantitative structure–activity relationship; IC50, the half maximal inhibitory concentration

References

(1) Choudhary, S., Kishore, N., and Hosur, R. V. (2015) Inhibition of insulin fibrillation by osmolytes: Mechanistic Insights. *Sci. Rep. 5*, 17599.

(2) Chen, Y., Ding, F., Nie, H., Serohijos, A. W., Sharma, S., Wilcox, K. C., Yin, S., and Dokholyan, N. V. (2008) Protein folding: then and now. *Arch. Biochem. Biophys. 469*, 4–19.

(3) Hartl, F. U., and Hayer-Hartl, M. (2009) Converging concepts of protein folding in vitro and in vivo. *Nat. Struct. Mol. Biol. 16*, 574–581.

(4) Dobson, C. M. (2003) Protein folding and misfolding. *Nature 426*, 884–890.

(5) Englander, S. W., Mayne, L., and Krishna, M. M. G. (2007) Protein folding and misfolding: mechanism and principles. *Q. Rev. Biophys. 40*, 287–326.

(6) Carrell, R. W., and Lomas, D. A. (1997) Conformational disease. *Lancet 350*, 134–138.

(7) Soto, C., and Estrada, L. D. (2008) Protein Misfolding and Neurodegeneration. *Arch. Neurol. 65*, 184–9.

(8) Chiti, F., and Dobson, C. M. (2006) Protein Misfolding, Functional Amyloid, and Human Disease. *Annu. Rev. Biochem. 75*, 333–366.

(9) Mucke, L., and Selkoe, D. J. (2012) Neurotoxicity of amyloid β-protein: synaptic and network dysfunction. *Cold Spring Harb. Perspect. Med. 2*, a006338.

(10) Makin, O. S., and Serpell, L. C. (2005) Structures for amyloid fibrils. *FEBS J. 272*, 5950–5961.

(11) Tycko, R. (2006) Molecular structure of amyloid fibrils: insights from solid-state NMR. *Q. Rev. Biophys. 39*, 1.

(12) Wälti, M. A., Ravotti, F., Arai, H., Glabe, C. G., Wall, J. S., Böckmann, A., Güntert, P., Meier, B. H., and Riek, R. (2016) Atomic-resolution structure of a disease-relevant Aβ(1-42) amyloid fibril. *Proc. Natl. Acad. Sci. U. S. A. 113*, E4976-84.

(13) Colvin, M. T., Silvers, R., Ni, Q. Z., Can, T. V., Sergeyev, I., Rosay, M., Donovan, K. J., Michael, B., Wall, J., Linse, S., and Griffin, R. G. (2016) Atomic Resolution Structure of Monomorphic $A\beta_{42}$ Amyloid Fibrils. *J. Am. Chem. Soc. 138*, 9663–9674.

(14) Ecroyd, H., and Carver, J. A. (2008) Unraveling the mysteries of protein folding and misfolding. *IUBMB Life 60*, 769–774.

(15) Knowles, T. P. J., Vendruscolo, M., and Dobson, C. M. (2014) The amyloid state and its association with protein misfolding diseases. *Nat. Rev. Mol. Cell Biol. 15*, 384–396.

(16) Lindgren, M., and Hammarström, P. (2010) Amyloid oligomers: spectroscopic characterization of amyloidogenic protein states. *FEBS J. 277*, 1380–1388.

(17) Kalhor, H. R., Kamizi, M., Akbari, J., and Heydari, A. (2009) Inhibition of Amyloid Formation by Ionic Liquids: Ionic Liquids Affecting Intermediate Oligomers. *Biomacromolecules 10*, 2468–2475.

(18) Xu, W., Su, H., Zhang, J. Z. H., and Mu, Y. (2012) Molecular Dynamics Simulation Study on the Molecular Structures of the Amylin Fibril Models. *J. Phys. Chem. B 116*, 13991–13999.

(19) Gong, H., He, Z., Peng, A., Zhang, X., Cheng, B., Sun, Y., Zheng, L., and Huang, K. (2015) Effects of several quinones on insulin aggregation. *Sci. Rep. 4*, 5648.

(20) Alam, P., Chaturvedi, S. K., Siddiqi, M. K., Rajpoot, R. K., Ajmal, M. R., Zaman, M., and Khan, R. H. (2016) Vitamin k3 inhibits protein aggregation: Implication in the treatment of amyloid diseases. *Sci. Rep. 6*, 26759.

(21) Li, W., Duan, X., Yan, H., Xin, H., Kelly, J. W., Sacchettini, J. C., Rossello, A., Freundich, J. S., Sacchettini, J. C., and Seibert, K. (2013) Synthesis of 4H-1,4-oxazines as transthyretin amyloid fibril inhibitors. *Org. Biomol. Chem. 11*, 4546.

(22) Swaminathan, R., Ravi, V. K., Kumar, S., Kumar, M. V. S., and Chandra, N. (2011) Lysozyme: A model protein for amyloid research. *Adv. Protein Chem. Struct. Biol.*, pp 63–111.

(23) Takai, E., Uda, K., Matsushita, S., Shikiya, Y., Yamada, Y., Shiraki, K., Zako, T., and Maeda, M. (2014) Cysteine inhibits amyloid fibrillation of lysozyme and directs the formation of small worm-like aggregates through non-covalent interactions. *Biotechnol. Prog. 30*, 470–478.

(24) Harte, N. P., Klyubin, I., McCarthy, E. K., Min, S., Garrahy, S. A., Xie, Y., Davey, G. P., Boland, J. J., Rowan, M. J., and Mok, K. H. (2015) Amyloid Oligomers and Mature Fibrils Prepared from an Innocuous Protein Cause Diverging Cellular Death Mechanisms. *J. Biol. Chem. 290*, 28343–52.

(25) Arosio, P., Vendruscolo, M., Dobson, C. M., and Knowles, T. P. J. (2014) Chemical kinetics for drug discovery to combat protein aggregation diseases. *Trends Pharmacol. Sci. 35*, 127–135.

(26) Kalhor, H. R., and Ashrafian, H. (2017) Identification of an aspidospermine derivative from borage extract as an anti-amyloid compound: A possible link between protein aggregation and antimalarial drugs. *Phytochemistry 140*, 134–140.

(27) Bu, X.-L., Rao, P. P. N., and Wang, Y.-J. (2016) Anti-amyloid Aggregation Activity of Natural Compounds: Implications for Alzheimer's Drug Discovery. *Mol. Neurobiol. 53*, 3565–3575.

(28) Mello, C. (2007) Return to the RNAi world: rethinking gene expression and evolution. *Cell Death Differ. 14*, 2013–2020.

(29) Sato, M., Murakami, K., Uno, M., Nakagawa, Y., Katayama, S., Akagi, K. -i., Masuda, Y., Takegoshi, K., and Irie, K. (2013) Site-specific Inhibitory Mechanism for Amyloid ?42 Aggregation by Catechol-type Flavonoids Targeting the Lys Residues. *J. Biol. Chem. 288*, 23212–23224.

(30) Evans, K. C., Berger, E. P., Cho, C. G., Weisgraber, K. H., Lansbury, P. T., and Jr. (1995) Apolipoprotein E is a kinetic but not a thermodynamic inhibitor of amyloid formation: implications for the pathogenesis and treatment of Alzheimer disease. *Proc. Natl. Acad. Sci. U. S. A. 92*, 763–7.

(31) Meng, F., Raleigh, D. P., and Abedini, A. (2010) Combination of Kinetically Selected Inhibitors *in Trans* Leads to Highly Effective Inhibition of Amyloid Formation. *J. Am. Chem. Soc. 132*, 14340–14342.

(32) Nakagami, Y., Nishimura, S., Murasugi, T., Kaneko, I., Meguro, M., Marumoto, S., Kogen, H., Koyama, K., and Oda, T. (2002) A novel β -sheet breaker, RS-0406, reverses amyloid β -induced cytotoxicity and impairment of long-term potentiation *in vitro*. *Br. J. Pharmacol. 137*, 676–682.

(33) O'Hare, E., Scopes, D. I. C., Treherne, J. M., Norwood, K., Spanswick, D., and Kim, E.-M.

(2010) RS-0406 Arrests Amyloid-β Oligomer-Induced Behavioural Deterioration In Vivo. *Behav. Brain Res. 210*, 32–37.

(34) Wermuth, C. G., Vergelli, C., Biancalani, C., Cesari, N., Graziano, A., Biagini, P., Gracia, J., Gavalda, A., Paz, V. D., Norton, C., Wen, J., Heise, C. E., Saunders, J., Conlon, P., Madan, A., Schwarz, D., and Goodfellow, V. S. (2011) Are pyridazines privileged structures? *Medchemcomm 2*, 935.

(35) Jaballah, M., Serya, R., and Abouzid, K. (2017) Pyridazine Based Scaffolds as Privileged Structures in anti-Cancer Therapy. *Drug Res. (Stuttg). 67*, 138–148.

(36) Pandiarajan, D., and Ramesh, R. (2012) μ-Halo bridged binuclear ruthenium(III) complexes featuring pyridazine ligands: Synthesis, structure, spectral and electrochemical properties. *Polyhedron 34*, 136–142.

(37) WO2010038081A2 - Heterocyclic derivatives and methods of use thereof - Google Patents.

(38) Kumar, S., Ravi, V. K., and Swaminathan, R. (2009) Suppression of lysozyme aggregation at alkaline pH by tri-N-acetylchitotriose. *Biochim. Biophys. Acta - Proteins Proteomics 1794*, 913–920.

(39) Kalhor, H. R., Kamizi, M., Akbari, J., and Heydari, A. (2009) Inhibition of Amyloid Formation by Ionic Liquids: Ionic Liquids Affecting Intermediate Oligomers. *Biomacromolecules 10*, 2468–2475.

(40) Pushpa Latha, P. D., and Sundara Sharmila, J. D. (2010) QSAR study for the prediction of IC50 and Log P for 5-N-Acetyl-Beta-D- Neuraminic Acid structurally similar compounds using stepwise (multivariate) linear regression. *Int. J. Chem. Res. 2*, 975–3699.

(41) Moghaddam, F. M., Pourkaveh, R., and Karimi, A. (2017) Oxidative Heck Reaction as a Tool for Para-selective Olefination of Aniline: A DFT Supported Mechanism. *J. Org. Chem. 82*, 10635–10640.

(42) Masaki Meguro,Tomiichiro Oda,Yasuhiro Nakagami, Shinji Marumoto, Kazuo Koyama, Isao Kaneko, Preventives or remedies for Alzheimer's disease, or amyloid protein fibril-formation inhibitors, which include a nitrogen-containing heteroaryl compound. US10497183. (2002)

(43) Mohammadi, F., Mahmudian, A., Moeeni, M., Hassani, L., Ho, Y. S., Hsieh, C. Y., Lin, J. K., McNeill, J. H., Orvig, C., Frautschy, S. A., and Cole, G. M. (2016) Inhibition of amyloid fibrillation of hen egg-white lysozyme by the natural and synthetic curcuminoids. *RSC Adv. 6*, 23148–23160.

(44) Frare, E., Polverino de Laureto, P., Zurdo, J., Dobson, C. M., and Fontana, A. (2004) A Highly Amyloidogenic Region of Hen Lysozyme. *J. Mol. Biol. 340*, 1153–1165.

(45) Mishima, T., Ohkuri, T., Monji, A., Imoto, T., and Ueda, T. (2007) A particular hydrophobic cluster in the residual structure of reduced lysozyme drastically affects the amyloid fibrils formation. *Biochem. Biophys. Res. Commun. 356*, 769–772.

(46) Wermuth, C. G. (2011) Are pyridazines privileged structures? *Medchemcomm 2*, 935.

(47) Schneider, W. C. (1948) The Dipole Moments of Diazines. *J. Am. Chem. Soc. 70*, 627–630.

(48) Frisch, M. J.; Trucks, G. W.; Schlegel, H. B.; Scuseria, G. E.; Robb, M. A.; Cheeseman, J. R.; Montgomery, J. A., Jr.; Vreven, T.; Kudin, K. N.; Burant, J. C.; Millam, J. M.; Iyengar, S. S.; Tomasi, J.; Barone, V.; Mennucci, B.; Cossi, M.; Scalmani, G.; Rega, N.; Petersson, G. A.;

Nakatsuji, H.; Hada, M.; Ehara, M.; Toyota, K.; Fukuda, R.; Hasegawa, J.; Ishida, M.; Nakajima, T.; Honda, Y.; Kitao, O.; Nakai, H.; Klene, M.; Li, X.; Knox, J. E.; Hratchian, H. P.; Cross, J. B.; Bakken, V.; Adamo, C.; Jaramillo, J.; Gomperts, R.; Stratmann, R. .; Yazyev, O.; Austin, A. J.; Cammi, R.; Pomelli, C.; Ochterski, J. W.; Ayala, P. Y.; Morokuma, K.; Voth, G. A.; Salvador, P.; Dannenberg, J. J.; Zakrzewski, V. G.; Dapprich, S.; Daniels, A. D.; Strain, M. C.; Farkas, O.; Malick, D. K.; Rabuck, A. D.; Raghavachari, K.; Foresman, J. B.; Ortiz, J. V.; Cui, Q.; Baboul, A. G.; Clifford, S.; Cioslowski, J.; Stefanov, B. B.; Liu, G.; Liashenko, A.; Piskorz, P.; Komaromi, I.; Martin, R. L.; Fox, D. J.; Keith, T.; Al-Laham, M. A.; Peng, C. Y.; Nanayakkara, A.; Challacombe, M.; Gill, P. M. W.; Johnson, B.; Chen, W.; Wong, M. W.; Gonzalez, C.; Pople, J. A. Gaussian 03, revision C.02; Gaussian, Inc.: Wallingford, CT, 2004.

(49) Kayed, R., Head, E., Thompson, J. L., McIntire, T. M., Milton, S. C., Cotman, C. W., and Glabe, C. G. (2003) Common Structure of Soluble Amyloid Oligomers Implies Common Mechanism of Pathogenesis. *Science (80-.). 300*, 486–489.

(50) Pilkington, E. H., Lai, M., Ge, X., Stanley, W. J., Wang, B., Wang, M., Kakinen, A., Sani, M.-A., Whittaker, M. R., Gurzov, E. N., Ding, F., Quinn, J. F., Davis, T. P., and Ke, P. C. (2017) Star Polymers Reduce Islet Amyloid Polypeptide Toxicity via Accelerated Amyloid Aggregation. *Biomacromolecules 18*, 4249–4260.

(51) Ferrari, E., Benassi, R., Saladini, M., Orteca, G., Gazova, Z., and Siposova, K. (2017) *In vitro* study on potential pharmacological activity of curcumin analogues and their copper complexes. *Chem. Biol. Drug Des. 89*, 411–419.

(52) Zhao, J., Wang, P., Li, H., and Gao, Z. (2015) Nitration of Y10 in $A\beta_{1–40}$: Is It a Compensatory Reaction against Oxidative/Nitrative Stress and Aβ Aggregation? *Chem. Res.*

Toxicol. 28, 401–407.

(53) Sayre LM1, Zagorski MG, Surewicz WK, Krafft GA, Perry G. (1997) Mechanisms of neurotoxicity associated with amyloid beta deposition and the role of free radicals in the pathogenesis of Alzheimer's disease: a critical appraisal. Chem Res Toxicol.;10(5):518-26.

(54) Kalhor, H. R., and Jabbari, M. P. (2017) Inhibition Mechanisms of a Pyridazine-Based Amyloid Inhibitor: As a β-Sheet Destabilizer and a Helix Bridge Maker. *J. Phys. Chem. B 121*, 7633–7645.

(55) Ramshini, H., Mannini, B., Khodayari, K., Ebrahim-Habibi, A., Moghaddasi, A. S., Tayebee, R., and Chiti, F. (2016) Bis(indolyl)phenylmethane derivatives are effective small molecules for inhibition of amyloid fibril formation by hen lysozyme. *Eur. J. Med. Chem. 124*, 361–371.

(56) Wilcken, R., Zimmermann, M. O., Lange, A., Joerger, A. C., and Boeckler, F. M. (2013) Principles and Applications of Halogen Bonding in Medicinal Chemistry and Chemical Biology. *J. Med. Chem. 56*, 1363–1388.

(57) Ibrahim, M. A. A. (2011) Molecular mechanical study of halogen bonding in drug discovery. *J. Comput. Chem. 32*, 2564–2574.

(58) Ferreira de Freitas, R., and Schapira, M. (2017) A systematic analysis of atomic protein–ligand interactions in the PDB. *Medchemcomm 8*, 1970–1981.

(59) Loureiro, J. A., Crespo, R., B?rner, H., Martins, P. M., Rocha, F. A., Coelho, M., Pereira, M. C., and Rocha, S. (2014) Fluorinated beta-sheet breaker peptides. *J. Mater. Chem. B 2*, 2259–2264.

(60) Palakurti, R., and Vadrevu, R. (2017) Pharmacophore based 3D-QSAR modeling, virtual screening and docking for identification of potential inhibitors of β-secretase. *Comput. Biol. Chem. 68*, 107–117.

Table 1

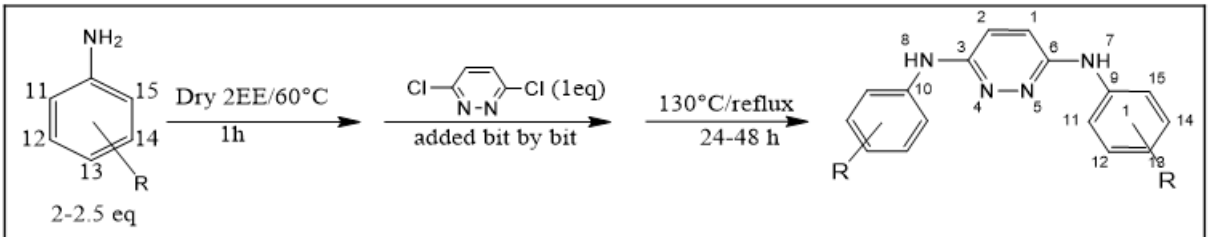

Entry	R	Time(h)	Yield(%)
Py-1	12-OH	24	85
Py-2	13-OH	24	72
Py-3	12-OCH_3	28	78
Py-4	——	28	57
Py-5	13-Br	48	68
Py-6	12,13-Cl	48	55
Py-7	12-F	48	29
Py-8	12-NO_2	48	30
Py-9	12-Cl	48	20
Py-10	13-Cl	48	45
Py-11	13-$COCH_3$	48	25
Py-12	13-NO_2	48	30
Py-13	13-F	48	15
Py-14	12-CH_3	48	39
Py-15	13-COOH	24[a]	93[a]
		20[b]	48[b]

Table 2

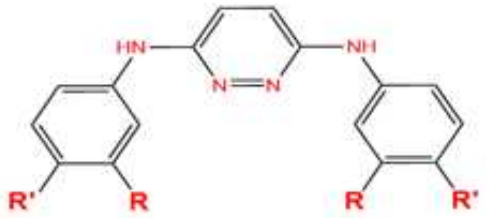

COM.	R	R'	LOG IC50
PY-1	OH	H	1.58 [a]
PY-2	H	OH	2.23 [a]
PY-3	OCH_3	H	2.31 [a]
PY-4	H	H	2.38 [a]
PY-5	H	Br	2.41 [a]
PY-6	Cl	Cl	3.91 [a]
PY-7	F	H	2.29 [a]
PY-8	NO_2	H	2.90 [a]
PY-9	Cl	H	2.50 [a]
PY-10	H	Cl	2.80 [a]
PY-15	**H**	**COOH**	**1.09** [b]
PY-16	**COOH**	**H**	**1.43** [b]

Fig. 1

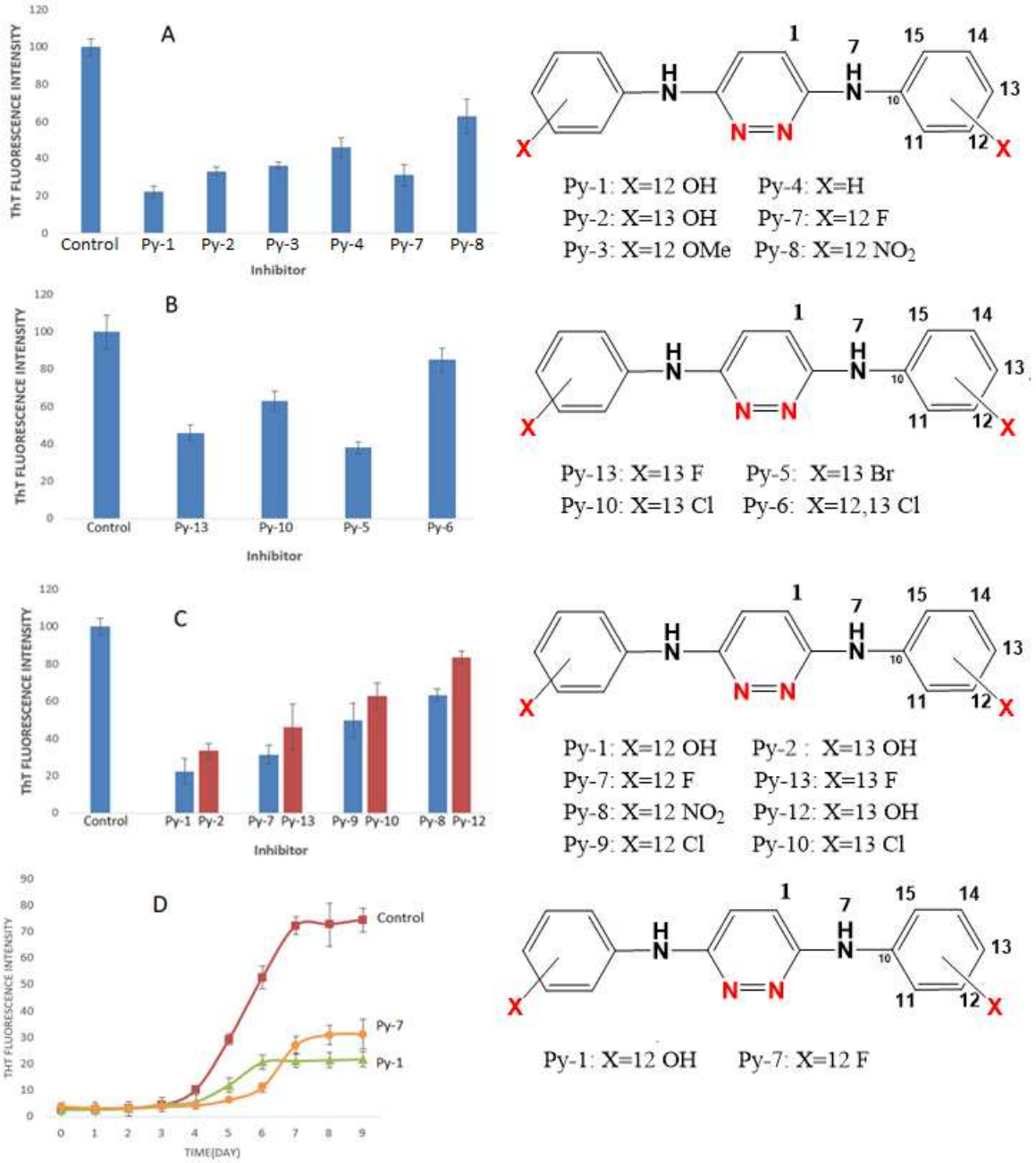
A
ThT FLUORESCENCE INTENSITY
Control
Py-1
Py-2
Py-3
Py-4
Py-7
Py-8
Inhibitor
Py-1: X=12 OH
Py-4: X=H
Py-2: X=13 OH
Py-7: X=12 F
Py-3: X=12 OMe
Py-8: X=12 NO2
B
Py-13
Py-10
Py-5
Py-6
Py-13: X=13 F
Py-5: X=13 Br
Py-10: X=13 Cl
Py-6: X=12,13 Cl
C
Py-9
Py-12
Py-1: X=12 OH
Py-2 : X=13 OH
Py-7: X=12 F
Py-13: X=13 F
Py-8: X=12 NO2
Py-12: X=13 OH
Py-9: X=12 Cl
Py-10: X=13 Cl
D
THT FLUORESCENCE INTENSITY
TIME(DAY)
Py-1: X=12 OH
Py-7: X=12 F

Fig. 2

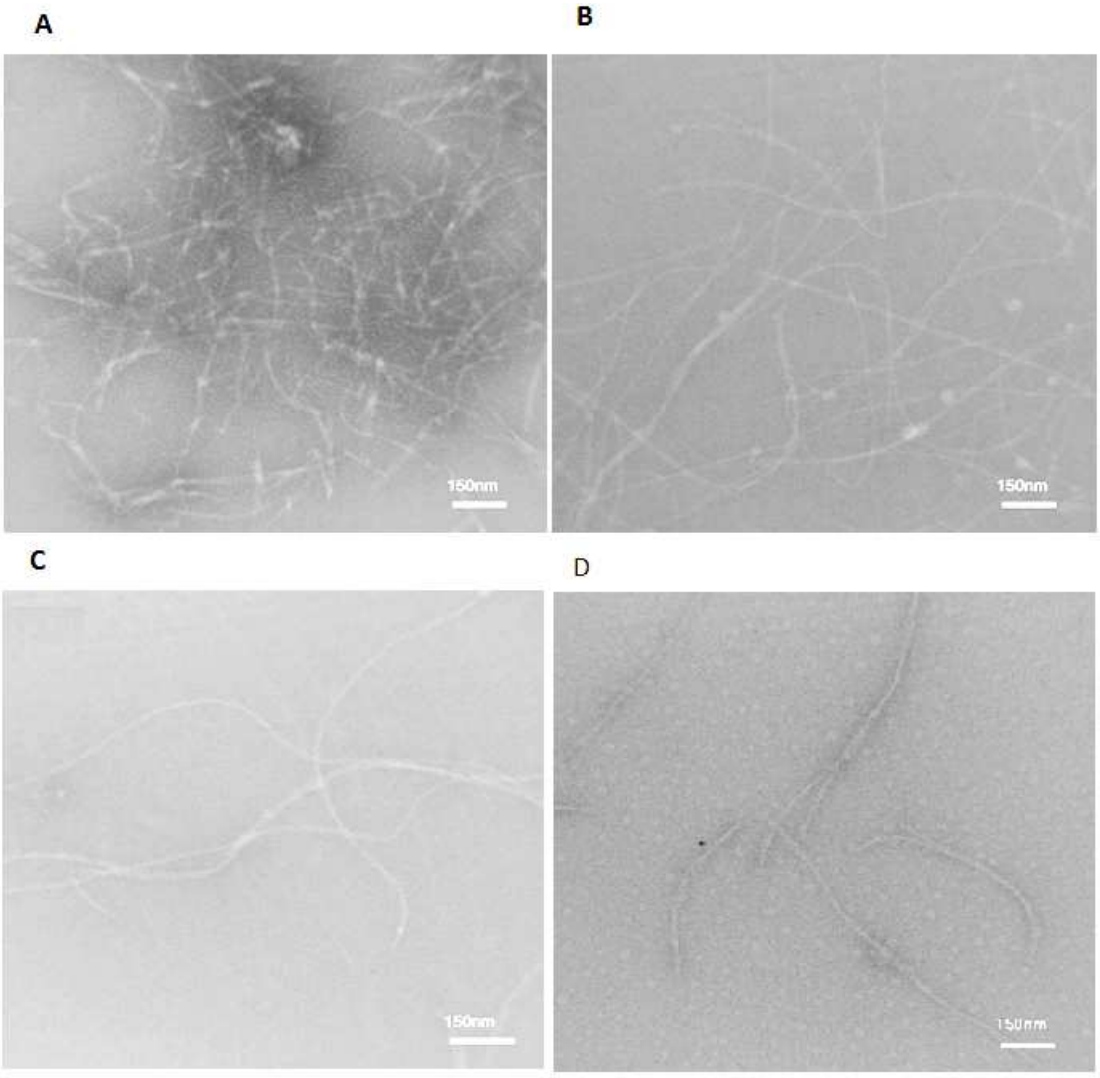

Fig. 3

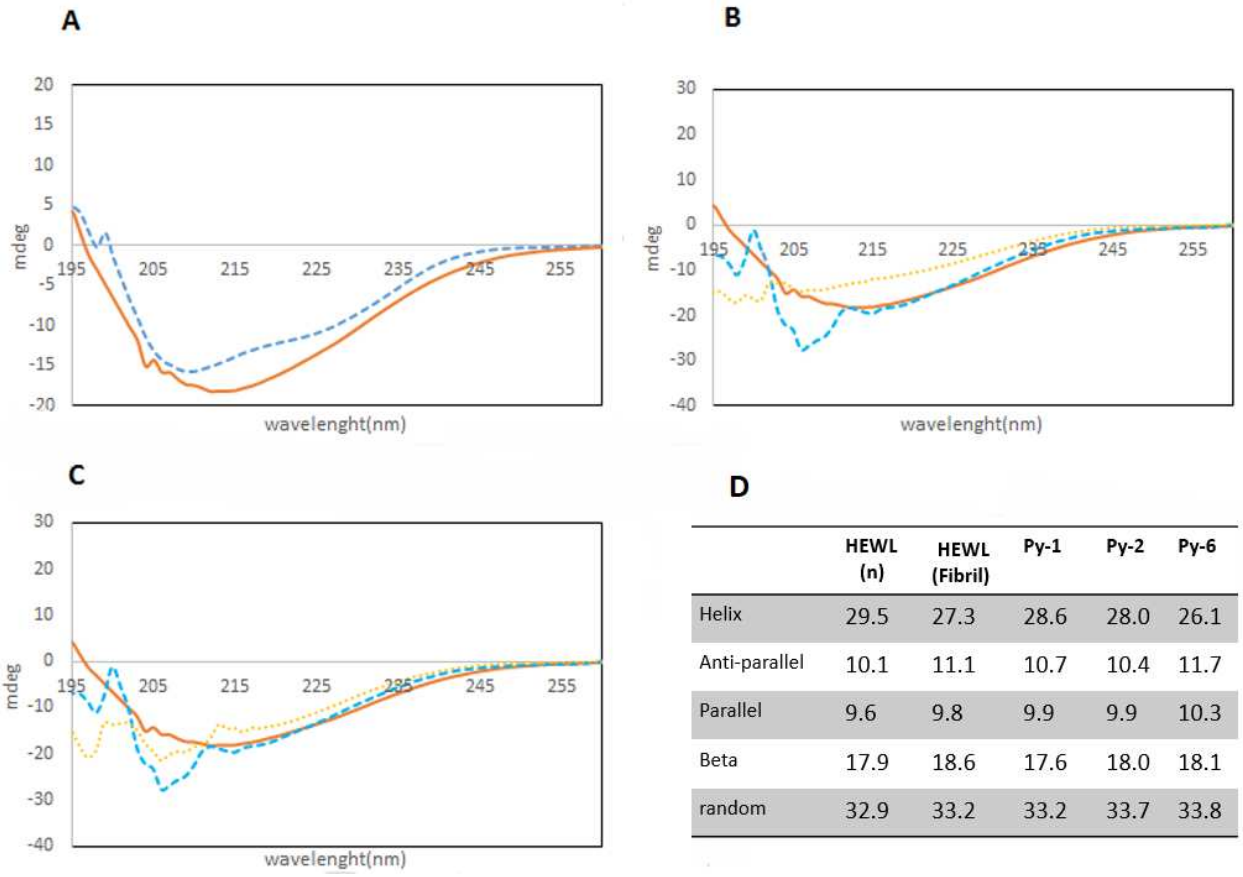

D

	HEWL (n)	HEWL (Fibril)	Py-1	Py-2	Py-6
Helix	29.5	27.3	28.6	28.0	26.1
Anti-parallel	10.1	11.1	10.7	10.4	11.7
Parallel	9.6	9.8	9.9	9.9	10.3
Beta	17.9	18.6	17.6	18.0	18.1
random	32.9	33.2	33.2	33.7	33.8

Fig. 4

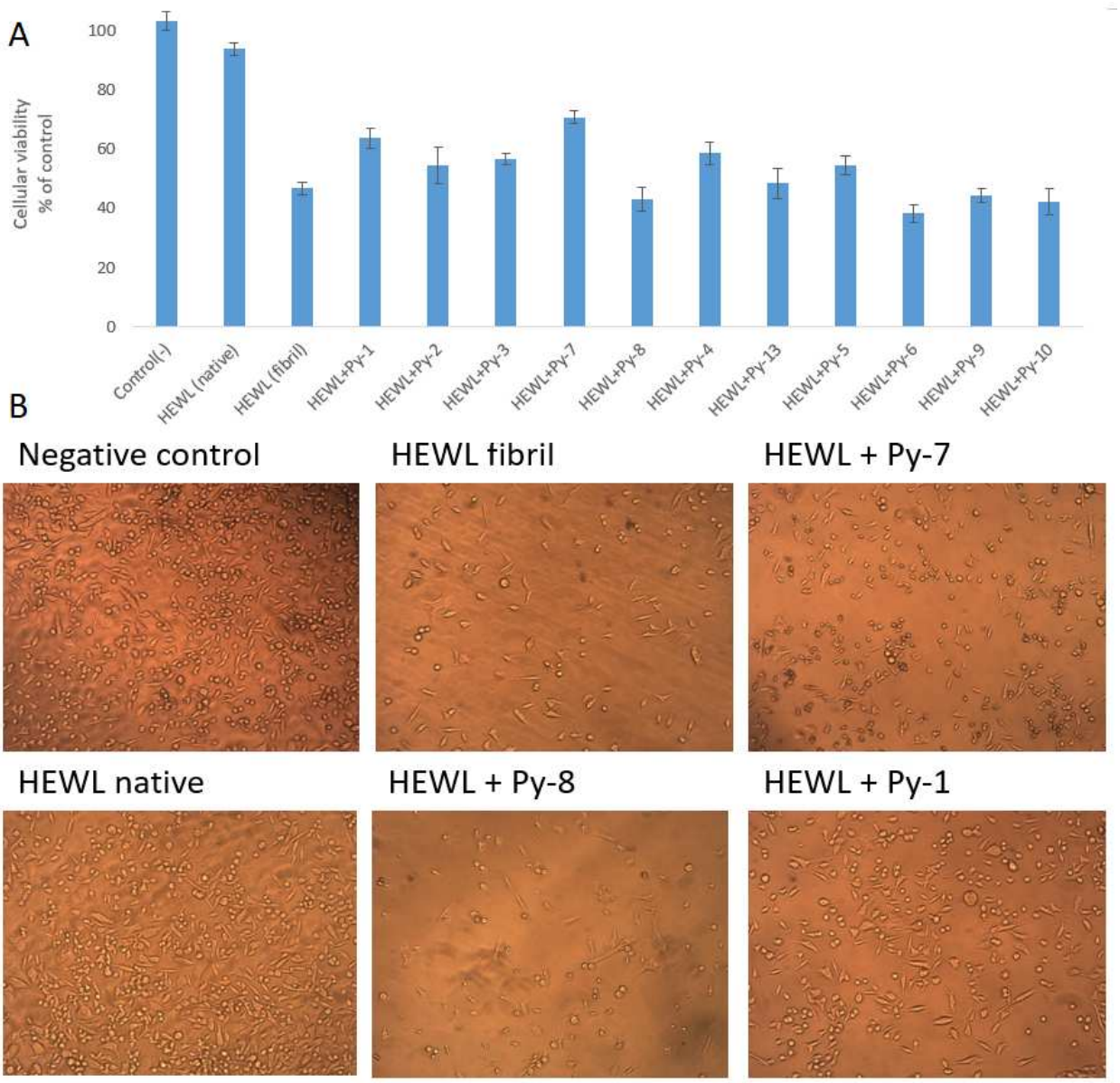
A
Cellular viability
% of control
100
80
60
40
20
0
Control(-)
HEWL (native)
HEWL (fibril)
HEWL+Py-1
HEWL+Py-2
HEWL+Py-3
HEWL+Py-7
HEWL+Py-8
HEWL+Py-4
HEWL+Py-13
HEWL+Py-5
HEWL+Py-6
HEWL+Py-9
HEWL+Py-10
B
Negative control
HEWL fibril
HEWL + Py-7
HEWL native
HEWL + Py-8
HEWL + Py-1

Fig. 5

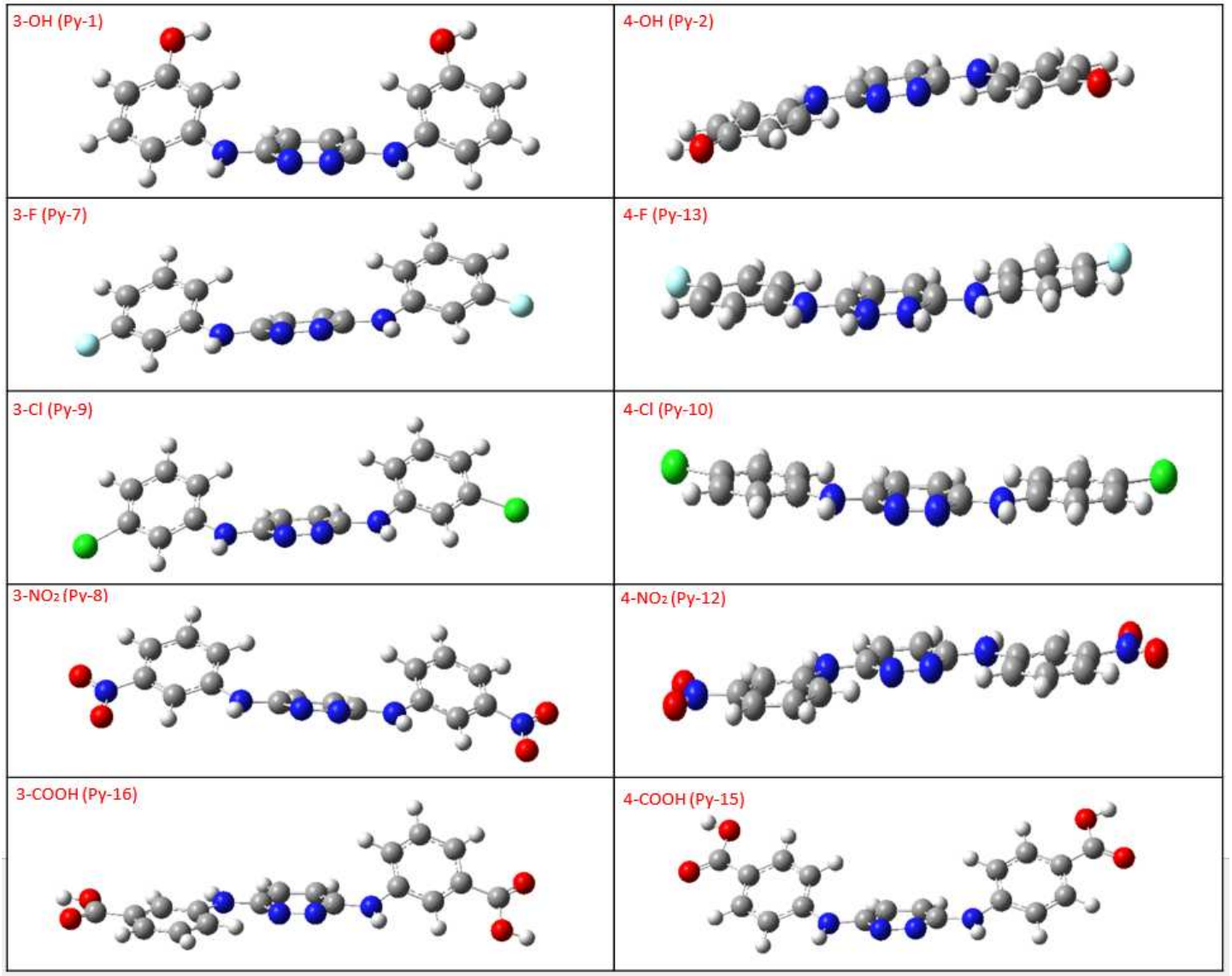
3-OH (Py-1)
4-OH (Py-2)
3-F (Py-7)
4-F (Py-13)
3-Cl (Py-9)
4-Cl (Py-10)
3-NO2 (Py-8)
4-NO2 (Py-12)
3-COOH (Py-16)
4-COOH (Py-15)

Fig. 6

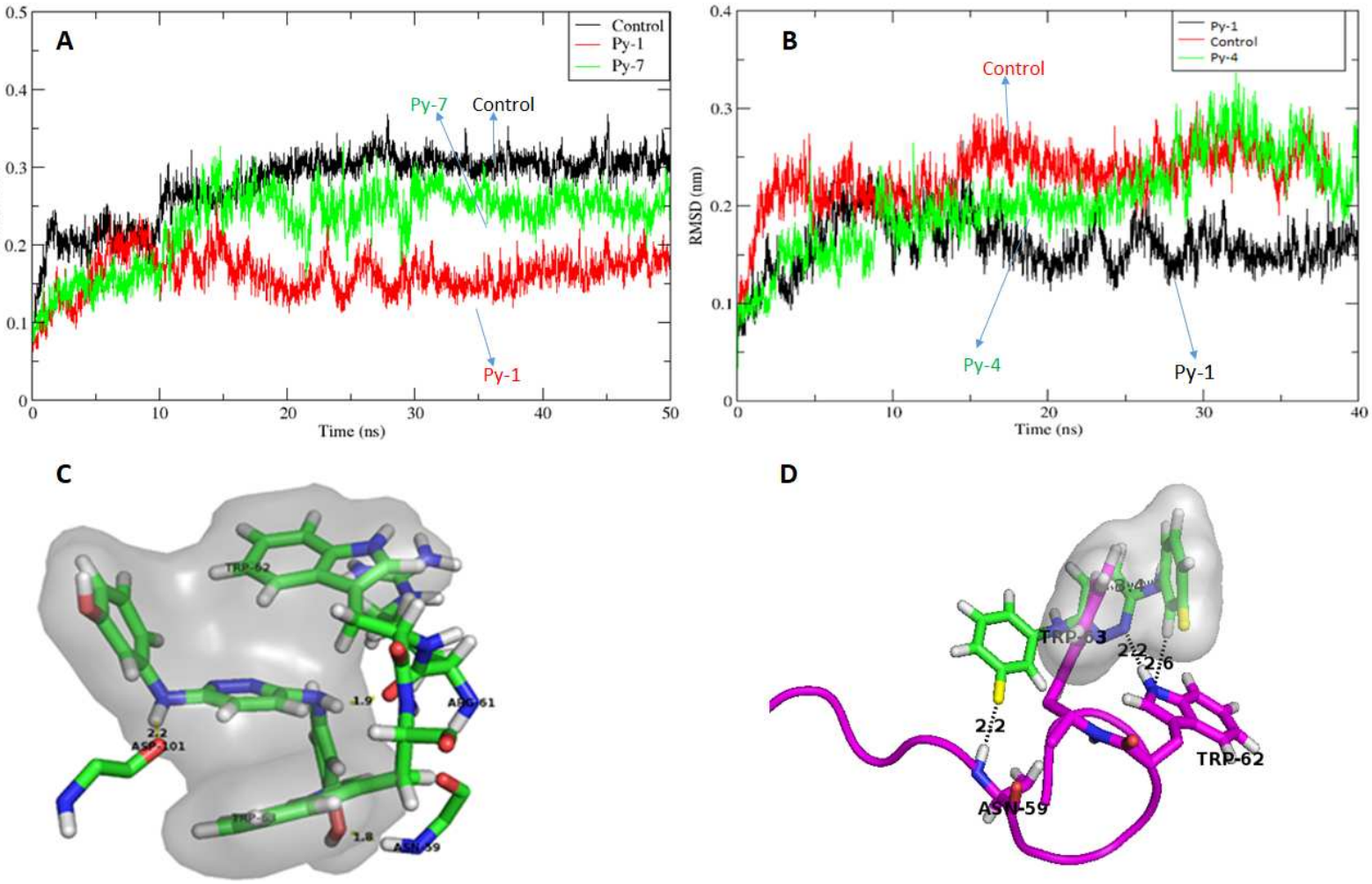
A
Control
Py-1
Py-7
Py-7
Control
Py-1
RMSD (nm)
Time (ns)
B
Py-1
Control
Py-4
Control
Py-4
Py-1
RMSD (nm)
Time (ns)
C
TRP-62
ASP-61
ASP-101
ASP-59
D
TRP-63
TRP-62
ASN-59

Legends:

Table 1. Reaction conditions and the yields for the pyridazine-based compounds synthesized in the present work. (a) The first method of synthesis was used. (b) The second method of synthesis was applied.

Table 2. IC50 values for the pyridazine-based compounds. (a) Values measured directly from experiments (b) Values predicted by QSAR method.

Figure 1. Th-T binding assay using synthetic compounds as inhibitors against HEWL amyloid fibrillation. Amyloid aggregation assay was set using HEWL (349 μM) in the presence of an inhibitor (349 μM) or no inhibitor (DMSO in same v/v %) as control. During fibrillation, samples were removed every 24 h, and Th-T emission was measured. (A) The effects of hydrogen-bonding on the aryl ring in amyloid fibril inhibition. (B) Effect of position of substitution (on the aryl ring) in amyloid fibril inhibition (C) Effect of bulkiness and halogen-binding of substitution of aryl ring in amyloid fibril formation (D) Kinetic inhibition of HEWL amyloid fibril formation using pyridazine-based compounds.

Figure 2. TEM images of HEWL fibril at 216 h (A) Control (in absence of any inhibitor), (B) In the presence of Py-6, (C) In the presence of Py-1, and (D) In the presence of Py-7.

Figure 3. Far-UV CD spectra HEWL fibrillation. (A) In the absence of any inhibitor at various time points: 0 h (----) and 216 h (—). (B) In the presence of inhibitors at 216 h: Py-1 (----), Py-6 (….) and control (—). (C) In the presence of inhibitors at 216 h: Py-1 (----), Py-2 (….) and control (—) (D) The secondary structure contents of HEWL.

Figure 4. Cell viability (MTT) assay, (A) Cytotoxicity of preformed aggregates of HEWL in the absence or presence of inhibitor. (B) Cell morphology of PC12 cells in the absence and the presence of preformed fibril of HEWL.

Figure 5. Optimized structure of pyridazine-based compounds. The computation has been done by Gaussian 3.0 and Gaussview 3.0, Density functional theory (DFT) method and optimization employing hybrid-functional B3LYP with 6-31+G (d) basis set.

Figure 6. The effects of inhibitors on HEWL aggregation using molecular dynamics (A) RMSDs of the lysozyme without any inhibitor (control) and in the presence of docked Py-1 and Py-7 (B) RMSDs of HEWL without any inhibitor and HEWL in the presence of docked Py-1or Py-7 (C) Snapshot during simulation of HEWL docked with Py-1.and (D) HEWL docked with Py-7.